Eur. Phys. J. A (2024) 60:140
https://doi.org/10.1140/epja/s10050-024-01362-y

THE EUROPEAN PHYSICAL JOURNAL A

Regular Article - Experimental Physics

High-resolution laser spectroscopy on the hyperfine structure and isotope shift of ^{237,239}Np

Magdalena Kaja[1,a], **Mitzi Urquiza-González**[2,3], **Felix Berg**[4], **Tobias Reich**[4], **Matou Stemmler**[1], **Dominik Studer**[5,6], **Felix Weber**[1], **Klaus Wendt**[1]

[1] Institute of Physics, Johannes Gutenberg University Mainz, Mainz 55099, Germany
[2] Division Hübner Photonics, Hübner GmbH & Co. KG, Kassel 34123, Germany
[3] Department of Physics, University of Gothenburg, Gothenburg SE-41296, Sweden
[4] Department of Chemistry—Nuclear Chemistry, Johannes Gutenberg University Mainz, Mainz 55099, Germany
[5] GSI Helmholtzzentrum für Schwerionenforschung GmbH, Darmstadt 64291, Germany
[6] Helmholtz Institute Mainz, Mainz 55099, Germany

Received: 18 March 2024 / Accepted: 14 June 2024 / Published online: 1 July 2024

Communicated by Klaus Blaum

Abstract Nuclear ground state properties of ^{237,239}Np were investigated by high-resolution laser spectroscopy at the RISIKO mass separator off-line radioactive beam facility of the University of Mainz. The isotope shifts and the hyperfine parameters were determined in two different atomic ground-state transitions at 398.80 nm and 395.61 nm. The data allowed for calculation of the so far unknown nuclear moments of the short-lived isotope ^{239}Np, i.e. the nuclear magnetic dipole moment of $\mu_I = +3.18(2)\,\mu_N$ and the electric quadrupole moment of $Q_S = +4.05(8)\,e$b, using the known nuclear moments of ^{237}Np as a reference, which were determined by electron paramagnetic resonance and investigations of muonic X-ray hyperfine structures, respectively.

1 Introduction

Nuclear ground state properties such as spin and electromagnetic moments as well as variations in mean square charge radii within an isotopic chain are highly relevant parameters to describe nuclear shell effects and deformations all along the nuclear chart and can serve as sensitive tests for nuclear models [1]. They can be determined with great precision using high-resolution laser spectroscopy [2]. This technique, which resolves the minor effects of hyperfine structures and isotope shifts in the optical resonance lines, has been refined in recent years towards both, remarkable precision as well as high sensitivity for studying minute sample sizes. Today, not only stable but also short-lived and exotic isotopes generated at various radioactive ion-beam facilities and nuclear reactors are accessible [1,3]. A specific region of interest for application of high-resolution laser spectroscopy is found in the range of the heaviest elements of the Periodic Table, i.e. the actinides and transactinides, where the stability of nuclear matter relies significantly on stabilizing shell effects. On the other hand, experimental data in this range of the nuclear chart, which would also validate theoretical estimates towards the description of the superheavy elements, are very scarce. Here we report on studies on the actinide element neptunium using resonance ionization mass spectrometry (RIMS). This technique has recently been adapted for high-resolution applications on rare radioisotopes [4] and has specifically been applied to actinides, both on-line [5] and off-line [6].

With an atomic number of Z = 93, neptunium is the first transuranium element. Naturally, it is occurring only in trace amounts as decay products from transmutation reactions in uranium ores. McMillan and Abelson discovered neptunium in 1939 [7] by subjecting ^{238}U to neutron bombardment. This led to the formation of the short-lived isotope ^{239}Np ($t_{1/2}$ = 2.356 d), which decays to ^{239}Pu. Two years later, the significantly longer-lived neptunium isotope ^{237}Np ($t_{1/2} = 2.1 \cdot 10^6$ y) was initially produced by Wahl and Seaborg through the bombardment of ^{238}U with fast neutrons [8]. Today, Np isotopes are a dominant by-product of the nuclear fuel cycle with the production of ~10 kg of ^{237}Np in each conventional pressurized water reactor annually [9]. Moreover, about 3 tons of ^{237}Np were released globally by mankind into the environment by above-ground nuclear detonations in the late 20th century [10]. Due to the very long half-life of ^{237}Np, it is essential to monitor nuclear waste repositories and their long-term performance specifically regarding ^{237}Np, which

[a] e-mail: mkaja@uni-mainz.de (corresponding author)

serves as an additional second motivation for the spectroscopic work described here.

The technique of RIMS, applied here for investigation of nuclear ground state properties in Np, has proven to be also suited as a sensitive and selective non-radiometric analytical technique for ultra-trace analytics in actinides and specifically ^{237}Np [11–13]. ^{239}Np could serve as a suitable tracer for precise quantification, which can be obtained as the alpha-decay daughter of ^{243}Am or alternatively from neutron irradiation of ^{238}U. However, its short half-life makes it an expensive and time-consuming option, as it has to be prepared and standardized on a weekly basis [14]. Its application in RIMS analytics thus relies on identifying ionization schemes with high elemental selectivity and the identification of isotope-related effects like hyperfine structures (HFS) and isotope shift (IS). Due to the large splittings and shifts observed in neptunium [15], unlike to most other elements, this becomes particularly important.

Already in 1977, a notable number of optical transitions in neptunium were categorized and hyperfine structure parameters for some of them were determined by Fred et al. [15]. Their experimental setup involved the analysis of a Np discharge at the 9 m Paschen-Runge spectrograph at Argonne National Laboratory together with Fourier transform spectroscopy at the Laboratoire Aime Cotton at Orsay. The precision of the HFS parameters $\mathcal{A}$ and $\mathcal{B}$ is not quoted in the paper. Considering the linewidths achieved by Fred et al. [15] of about 1 GHz, we estimated the errors to be in the order of 10 MHz for $\mathcal{A}$ and 300 MHz for $\mathcal{B}$. These estimates were obtained by fitting artificially generated data with this linewidth and suitable other parameters.

In this work, we report on two-step resonance ionization spectroscopy performed on both isotopes ^{237,239}Np. The high resolution was accomplished by using a perpendicularly illuminated laser ion source and trap (PI-LIST) unit at the off-line mass separator RISIKO of Mainz University [5,16]. The HFS for both isotopes was studied in two different atomic ground-state transitions, which allowed for the determination of the nuclear moments of ^{239}Np and the extraction of the isotope shift between ^{237}Np and ^{239}Np in these transitions.

2 Experimental setup

Neptunium samples were prepared at the Department of Chemistry - Nuclear Chemistry, TRIGA site of the University of Mainz. ^{237}Np was available as a stock solution, while ^{239}Np was produced by irradiation of ^{238}U at the research reactor TRIGA Mark II Mainz and chemically purified through anion exchange column chromatography as described in [17]. Samples containing about 10^{13} atoms of ^{237}Np and 10^{11} atoms of ^{239}Np in nitric acid solution were deposited onto a 4 x 4 mm^2 zirconium carrier foil and evaporated slowly under an infrared lamp. As had been investigated in test measurements, Zr as a reduction agent combines optimum evaporation of Np atoms with good durability under high-temperature conditions. The folded foil was inserted into the atomizer cavity of the RISIKO mass separator ion source [18]. A simplified sketch giving the spectroscopy components of the setup up to the PI-LIST unit is presented in Fig. 1. The atomizer was resistively heated gradually up to an evaporation temperature with a maximum around 2000 °C, ensuring smooth evaporation of Np. The evaporated neutral atoms drift towards the front end of the cavity to enter the PI-LIST as an atomic beam, which is well suited for high-resolution spectroscopy. The PI-LIST has two repeller electrodes facing the atomizer and a radiofrequency quadrupole (RFQ) ion guide structure with a free field radius of 7.5 mm, a rod diameter of 10 mm, and a length of 45 mm. The repeller electrodes suppress background stemming from electrons emitted from the hot atomizer or surface ionized species. Inside the RFQ structure, the atomic beam is intersected by the beam of the spectroscopy laser entering the vacuum chamber through a window at the side of the ion source in a perpendicular geometry to substantially reduce Doppler broadening. The interaction region is located at a distance of just a few millimeters from the atomizer. To further reduce the Doppler width, the second laser beam, inducing the ionization transition is entering through a window in the mass separator magnet, in this way overlapping the atom beam in an anti-collinear manner. This configuration selects a narrow velocity class of atoms and narrows the effective opening angle within the interaction region to a minimum. A downside of this geometry is a reduction in ionization efficiency by a factor of about 100 compared to standard in-source laser ionization [16], for which this value is in the order of 10%. The ions created inside the RFQ structure are confined by the guiding RF field and transported towards the exit electrode of the PI-LIST to be accelerated to 30 keV. Subsequently, they undergo separation in the 60° sector field magnet based on their mass-to-charge ratio. In this process, adjacent masses are eliminated by a separator slit in the focal plane of the magnet. Typically a mass resolving power of $M/\Delta M \approx 600$ is realized. Finally, the ions are counted on a MagneTOF single ion detector. To further suppress background, time-resolved acquisition of the created ions was employed using a multichannel analyzer. Due to the pulsed laser ionization, the ion beam features a bunched structure with 20 μs width and 100 μs period. Counts from ions that are detected outside the expected time window are rejected, thus reducing the time-independent background by a factor of five.

Two different two-step resonant ionization schemes, labeled (A) and (B), were investigated in this work. Transition wavelengths, corresponding to the reciprocal of the wavenumber differences, are explicitly given in [19] as well as below in the text.

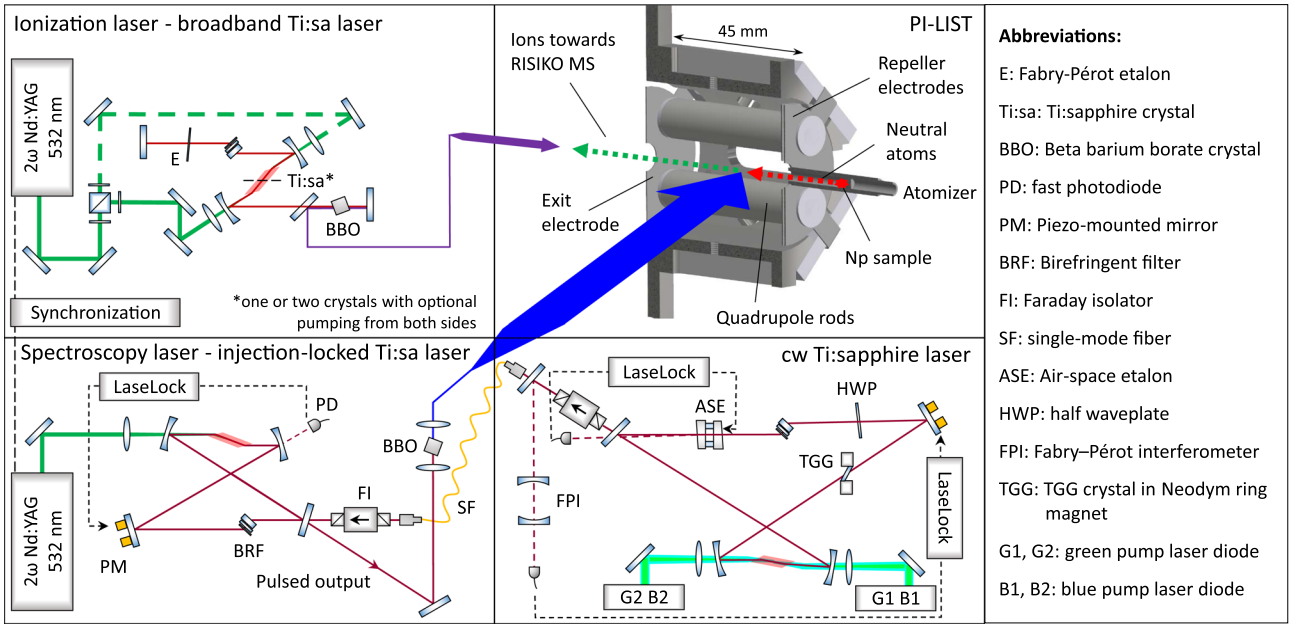

Fig. 1 Partial experimental sketch, including the pulsed broadband Ti:sapphire laser for the ionization, the pulsed injection-locked Ti:sa laser seeded by cw Ti:sapphire laser employed for spectroscopy, along with the PI-LIST ion source. Abbreviations are given in the legend on the right

(A) $0\,\mathrm{cm}^{-1} \rightarrow 25075.15\,\mathrm{cm}^{-1} \rightarrow 50813.6\,\mathrm{cm}^{-1}$
(B) $0\,\mathrm{cm}^{-1} \rightarrow 25277.64\,\mathrm{cm}^{-1} \rightarrow 50909.4\,\mathrm{cm}^{-1}$.

The ground state has an electron configuration $5f^4 6d 7s^2\ {}^6L_{11/2}$. For both first excited states, the detailed electron configuration is unknown, while the total angular momentum is known to be $J = 13/2$ for scheme (A) and $J = 9/2$ for scheme (B). The choice of the second step, in both cases leading to strong autoionizing levels just above the ionization potential of $\mathrm{IP_{Np}} = 50\,535.54(15)\ \mathrm{cm}^{-1}$ [19], took into account the presence of the daughter nuclide of ^{239}Np, i.e. ^{239}Pu, to guarantee for suitable elemental selectivity. The corresponding studies are detailed in a separate work [19]. The 398.80 nm and 395.61 nm for the first steps of schemes (A) and (B) were generated using the narrowband spectroscopy laser, namely, a pulsed injection-locked Ti:sapphire laser, arranged in a bow-tie configuration and delivering high power pulsed laser radiation with a bandwidth of about 20 MHz [20]. It was seeded by a custom-built direct diode-pumped cw Ti:sapphire laser [21,22]. To create the second harmonic, the laser light from the spectroscopy laser was focused into a BBO crystal placed outside the cavity for simple single-pass transmission. That resulted in an output power of about 100 mW. To enhance the spatial interaction volume with the effusing atomic beam, the laser beam of typical vertical height of 2 mm was expanded horizontally to approximately 2 cm in width in front of the PI-LIST, creating a large overlap area with the ionization laser beam of about 2 mm in diameter. A High Finesse WSU-30 wavelength meter was used for frequency measurements of the fundamental wavelengths. It was regularly calibrated to an ECDL, locked to the $F = 2 \rightarrow F' = 3$ transition in the D_2 line of ^{87}Rb near 780 nm via saturated absorption spectroscopy. A similar technique was used in high-resolution spectroscopy in Cf [6] and Pm [23]. The 388.52 nm for the ionizing step of the scheme (A) was generated using a standard Z-shaped Ti:sapphire laser with a spectral linewidth of 5 GHz, and a typical pulse length of 50 ns [24]. The laser light was frequency doubled by an intracavity frequency doubling process within a beta barium borate (BBO) crystal. That resulted in an output power of up to 1 W in the range of 360-400 nm. The 390.14 nm for the ionizing step of the scheme (B) was produced by a specific high-power Ti:sapphire laser equipped with two gain crystals delivering a laser power up to 3 W, while maintaining similar spectral, spatial, and temporal beam quality of a standard laser system. The lasers were pumped with 15 W, respective 30 W for the double crystal laser, of a Nd:YAG laser operating in frequency-doubled mode at 532 nm with a 10 kHz repetition rate.

3 High-resolution spectroscopy

The HFS of ^{237,239}Np and the isotope shift between these two isotopes were measured in the ground-state transitions of the two ionization schemes (A) and (B), as presented in Fig. 2. The nuclear spins of ^{237,239}Np are identical with $I = 5/2$. Because of the vector coupling of the angular momentum $\vec{J}$ of the atomic shell and this nuclear spin $\vec{I}$, according to $\vec{F} = \vec{J} + \vec{I}$, each one of the examined atomic states splits

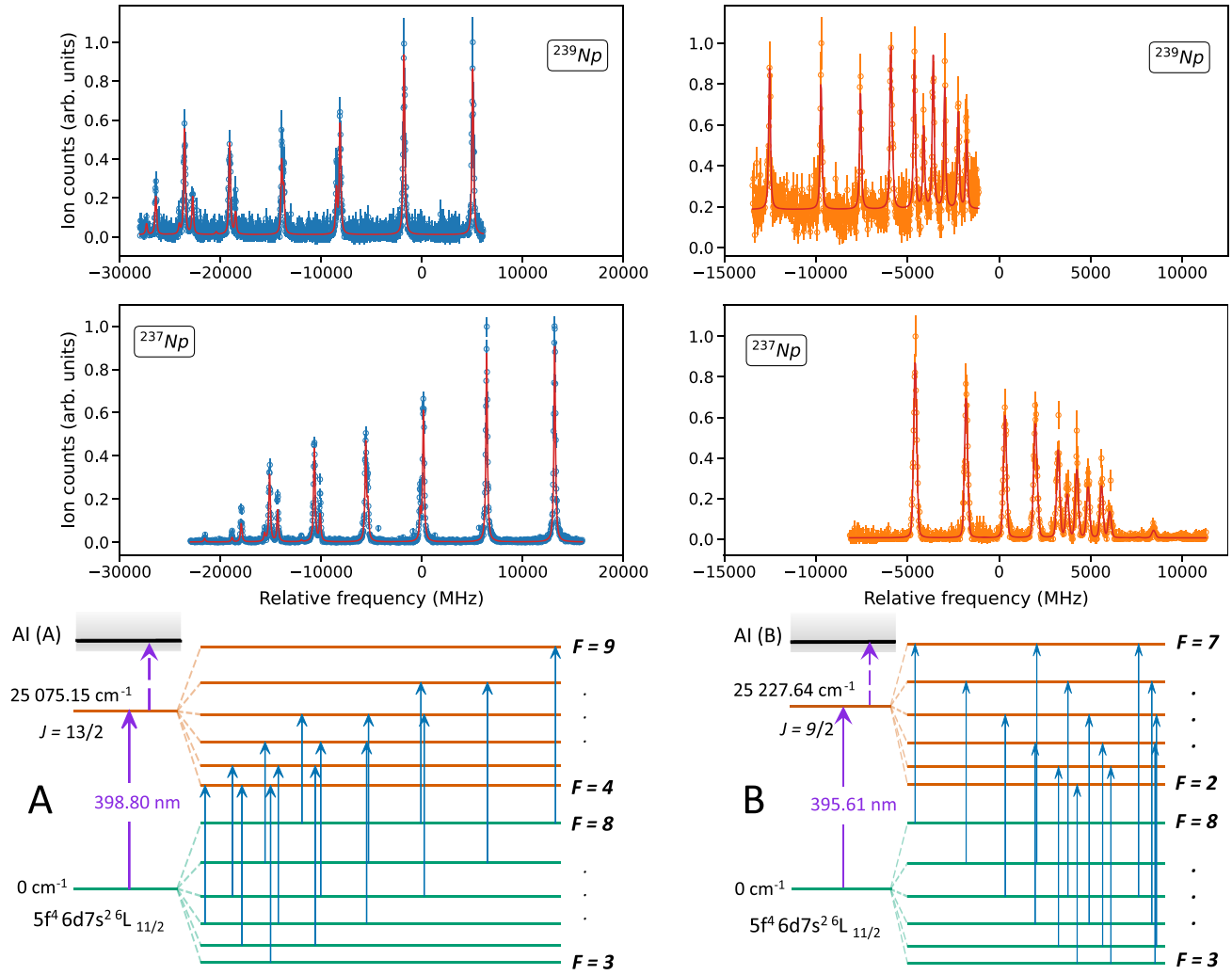

Fig. 2 Measured transitions for ^{237,239}Np. The hyperfine spectra in the ground state transition of scheme (**A**) at 399 nm on the left side and scheme (**B**) at 396 nm on the right. The hyperfine splitting of the atomic ground and respective first excited state are given below for ^{237}Np indicating the permitted hyperfine transitions by blue arrows. The Np ionization potential is $\mathrm{IP_{Np}} = 50\,535.54(15)\,\mathrm{cm}^{-1}$ [19]

into 6 HFS sub-levels with $|\ I - J\ | \leq F \leq I + J$. The energetic position of the hyperfine sub-levels is given by the HFS formula

$$\Delta E_{HFS} = \Delta E_{\mu} + \Delta E_{Q} = \frac{\mathcal{A}C}{2} + \frac{\mathcal{B}}{4}\frac{\frac{3}{2}C(C+1) - 2I(I+1)J(J+1)}{I(2I-1)J(2J-1)}, \quad (1)$$

where $C = F(F+1) - J(J+1) - I(I+1)$ [1].

This results in 15 permitted transitions between the ground and excited states, determined by the selection rules $\Delta F = 0, \pm 1$. For ^{239}Np, 10 lines were experimentally observed as well visible peaks in each scheme (A) and (B), whereas for ^{237}Np 13 and 11, respectively, were observed. The laser power of the spectroscopy laser was reduced to about 20 mW as it was tested to be a good compromise between efficiency and linewidth. The ionization laser was limited to about 450 mW to avoid background resulting from non-resonant ionization. The only exception was the measurement of ^{239}Np using scheme (B), where the laser power of the ionization laser was set to 3.5 W. This was necessary due to the slightly lower efficiency of this scheme and the limited amount of ^{239}Np in the sample. For the stronger transition at 398.80 nm in the scheme (A), a linewidth of approximately 190 MHz was recorded, whereas for the transition of 395.61 nm, it was about 120 MHz. Both linewidths could have been improved by further reducing the power in the spectroscopy laser, although this would have reduced statistics and impeded the observation of the smallest peaks.

The analysis of the spectra was performed using the SATLAS2 python package [25,26]. Line shapes were fitted with Voigt profiles and Racah coefficients were taken

Table 1 Extracted parameters for ^{237,239}Np isotopes for different atomic energy levels. The determined $\mathcal{A}_{exp}$ and $\mathcal{B}_{exp}$ parameters for ^{237}Np are compared with the previously reported values $\mathcal{A}_{lit}$ and $\mathcal{B}_{lit}$ from Ref. [15]

State	E (cm^{-1})	J	^{237}Np				^{239}Np	
			$\mathcal{A}_{exp}$	$\mathcal{B}_{exp}$	$\mathcal{A}_{lit}$	$\mathcal{B}_{lit}$	$\mathcal{A}_{exp}$	$\mathcal{B}_{exp}$
GS	0	11/2	776.08(20)	928(10)	778	645	785.59(39)	955(10)
FES$_A$	25 075.15	13/2	1470.09(18)	323(8)	1470	264	1487.43(34)	346(10)
FES$_B$	25 277.64	9/2	570.08(22)	-302(9)	–	–	577.01(47)	−311(11)

The errors of literature values were estimated by us to be in the order of 10 MHz for $\mathcal{A}$ and 300 MHz for $\mathcal{B}$ based on the 1 GHz linewidths, as discussed in the text. The HFS parameters are given in units of MHz

for initial line intensity settings. For the optimum match, the intensities were converted to free parameters after identification of the individual HFS components to account for contributions of optical hyperfine pumping and variations in the ion beam strength. The HFS parameters determined from the measured hyperfine spectra are summarized in Table 1. Three and two individual spectra per scheme were taken for ^{237}Np and ^{239}Np, respectively, and were jointly fitted with shared parameters of the ground state. The upper state parameters were also shared for the respective measurements of the same transition. A variation in the spin assignment from the expected values of 5/2 towards 3/2 or 7/2, respectively, for both isotopes was tested in the evaluation but did not lead to reasonable reproduction of either the HFS patterns or the extracted HFS parameters. Thus a nuclear spin of 5/2 was confirmed.

The obtained $\mathcal{A}$ parameters for ^{237}Np are in very good agreement with the values obtained by Fred et al. [15]. That is not the case for $\mathcal{B}$ parameters. However, a HFS simulation showed that for linewidths well above 1 GHz as accomplished by Fred et al., the finer structures of close-lying double peaks are not resolved. A simulated HFS structure with our parameters and that linewidth is almost indistinguishable from the HFS measured by Fred et al. explaining the large discrepancy in $\mathcal{B}$. Compared with each other, the HFS parameters of the ^{237,239}Np isotopes do almost not differ at all. This finding is well understood by the fact, that both isotopes share the same nuclear ground state configuration based upon the nuclear spin $I = 5/2^+$ and the similar Nilsson orbital [642]. A detailed discussion on this aspect is given in [27].

Regarding the nuclear ground state properties of Np, the nuclear moment was only known with reasonable precision for ^{237}Np so far. That nuclear magnetic dipole moment was determined using electron paramagnetic resonance to be $\mu_I = +3.14(4)\mu_N$, as recalibrated by Stone [28] from the original data of [29]. The electric quadrupole moment is $Q_S = +3.886(6)$ eb as derived from the studies of muonic X-ray hyperfine structures [30]. With these values, the nuclear moments for ^{239}Np were determined from the extracted HFS parameters of this work using the relations

$$\mu_I = \frac{\mathcal{A}}{\mathcal{A}_{ref}} \frac{I}{I_{ref}} \mu_{I,ref} \tag{2}$$

$$Q_s = \frac{\mathcal{B}}{\mathcal{B}_{ref}} Q_{s,ref} \tag{3}$$

with ^{237}Np as reference isotope, giving $\mu_I = +3.18(4)\mu_N$ and $Q_S = +4.05(2)$ eb. The values were determined from the three individual $\mathcal{A}$ and $\mathcal{B}$ factors, respectively, using the properly weighted average. As expected, the results are almost identical to the nuclear moments of ^{237}Np, confirming the almost perfectly identical nuclear structure of both isotopes, as pointed out in [27].

Another spectroscopic parameter affected by nuclear structure is the isotope shift, which represents the frequency shift $\delta\nu$ in an atomic transition i between the two isotopes with mass numbers A and A′,

$$\delta\nu_i^{A,A'} = \nu_i^{A'} - \nu_i^{A}. \tag{4}$$

Values for the two ground state transitions studied were extracted from the measured spectra to be $\delta\nu^{237,239}_{399\,\mathrm{nm}} = -8\,168(17)$ MHz and $\delta\nu^{237,239}_{396\,\mathrm{nm}} = -7\,892(13)$ MHz. The lower transition frequency of ^{239}Np compared to ^{237}Np indicates that most likely an s-p transition takes place in both cases, in which the s electron is more tightly bound in the smaller nucleus, which is known to be ^{237}Np due to the almost identical nuclear moments. For very heavy nuclei with $A > 200$ the isotope shift is predominantly caused by the change in the mean-squared charge radius $\delta\langle r^2\rangle = \delta\nu/F_{398/395}$ of the nucleus, while a mass shift effect, caused by the very small relative mass difference amounts to only a few ten MHz. The ratio is given by the electronic factor F of the corresponding atomic transition [1]. Due to the missing assignment for the two excited levels under study and, correspondingly, no suitable guess for the F-value, an extraction of the value of $\delta\langle r^2\rangle^{(237,239)}$ was not attempted. Furthermore, to our knowledge, there is no experimental or theoretical data on absolute charge radii of neptunium available. A future study, involving also additional isotopes on Np should thus aim for involving theoretical support on electronic factors as connection between atomic and nuclear parameters.

4 Conclusion and outlook

We conducted an investigation of the hyperfine spectra within two atomic ground state transitions of the neptunium isotopes ^{237}Np and ^{239}Np. This led to the precise determination of hyperfine parameters and isotope shifts. Furthermore, the magnetic dipole and electric quadrupole moments for the isotope ^{239}Np were determined with high accuracy for the first time, exhibiting a very weak and smooth development of nuclear shape. Through this work, we have laid a foundation for future high-resolution spectroscopic experiments at radioactive ion beam facilities targeting more exotic nuclei in the chain of Np isotopes and neighboring actinides, which are available only in on-line experiments. The PI-LIST ion source, which has recently undergone tests for online applications, holds promise for such studies [5]. Our findings are also valuable for RIMS measurements of neptunium contents in environmental samples by providing the necessary spectroscopic data for the prediction of line positions and hyperfine patterns from the determined nuclear moments and isotope shifts for the use of ^{239}Np as possible reference isotope for quantification.

Acknowledgements This work has received funding from the European Union's Horizon 2020 Research and Innovation Programme under grant agreement project number 861198 (LISA) Marie Sklodowska-Curie Innovative Training Network (ITN) and Federal Ministry of Education and Research (BMBF) under contract number 05P21UMFN3 and 02NUK075B (project SOLARIS).

Author contributions Conceptualization: MK, DS, FW, KW; Investigation: MK, MU-G, MS, DS, FW; formal analysis and visualization: MK; writing—original draft preparation: MK; writing—review and editing: MK, MU-G, FB, TR, DS, KW; funding acquisition: TR, KW; resources: FB; supervision: TR, KW.

Funding Open Access funding enabled and organized by Projekt DEAL.

Data Availibility Statement Data will be made available on reasonable request. [Author's comment: The datasets generated during and/or analysed during the current study are available from the corresponding author on reasonable request.]

Code Availibility Statement This manuscript has no associated code/software. [Author's comment: Code/Software sharing not applicable to this article as no code/software was generated or analysed during the current study.]

References

1. P. Campbell, I. Moore, M. Pearson, Progress Particle Nucl. Phys. **86**, 127 (2016)
2. W. Demtröder, *Laser Spectroscopy 2*, 5th edn. (Springer, Berlin, 2015). 978-3-662-44641-6
3. X. Yang, S. Wang, S. Wilkins, R.G. Ruiz, Progress Particle Nucl. Phys. **129**, 104005 (2023)
4. T. Kron, R. Beerwerth, S. Raeder, S. Fritzsche, R. Heinke, P. Schönberg, M. Trümper, K. Wendt, Phys. Rev. C **102**, 034307 (2020)
5. R. Heinke, M. Au, C. Bernerd, K. Chrysalidis, T.E. Cocolios, V.N. Fedosseev, I. Hendriks, A.A. Jaradat, M. Kaja, T. Kieck et al., Nuclear Instruments and Methods in Physics Research Section B: Beam Interactions with Materials and Atoms **541**, 8 (2023)
6. F. Weber, T.E. Albrecht-Schönzart, S.O. Allehabi, S. Berndt, M. Block, H. Dorrer, C.E. Düllmann, V.A. Dzuba, J.G. Ezold, V.V. Flambaum et al., Phys. Rev. C **107**, 034313 (2023)
7. E. McMillan, P.H. Abelson, Phys. Rev. **57**, 1185 (1940)
8. A.C. Wahl, G.T. Seaborg, Phys. Rev. **73**, 940 (1948)
9. M. Krachler, R. Alvarez-Sarandes, P. Souček, P. Carbol, Microchem. J. **117**, 225 (2014)
10. T. Beasley, J. Kelley, T. Maiti, L. Bond, J. Environ. Radioactivity **38**, 133 (1998)
11. H. Bosco, L. Hamann, N. Kneip, M. Raiwa, M. Weiss, K. Wendt, C. Walther, Science Advances **7** (2021)
12. J. Riegel, R. Deißenberger, G. Herrmann, S. Köhler, P. Sattelberger, N. Trautmann, H. Wendeler, F. Ames, H.J. Kluge, F. Scheerer et al., Appl. Phys. B Photophys. Laser Chem. **56**, 275 (1993)
13. S. Raeder, N. Stöbener, T. Gottwald, G. Passler, T. Reich, N. Trautmann, K. Wendt, Spectrochimica Acta Part B **66**, 242 (2011)
14. P. Thakur, G. Mulholland, Appl Radiation Isotopes **70**, 1747 (2012)
15. M. Fred, F.S. Tomkins, J.E. Blaise, P. Camus, J. Vergès, J Opt Soc Am **67**, 7 (1977)
16. R. Heinke, T. Kron, S. Raeder, T. Reich, P. Schönberg, M. Trümper, C. Weichhold, K. Wendt, Hyperfine Interactions **238** (2017)
17. S. Amayri, A. Jermolajev, T. Reich, Radiochimica Acta **99**, 349 (2011)
18. T. Kieck, H. Dorrer, C.E. Düllmann, V. Gadelshin, F. Schneider, K. Wendt, Nuclear Instruments and Methods in Physics Research Section A: Accelerators. Spectrometers Detectors Assoc Equipment **945**, 162602 (2019)
19. M. Kaja, D. Studer, F. Berg, S. Berndt, Ch.E. Düllmann, N. Kneip, T. Reich, M. Urquiza-González, K. Wendt, Euro Phys J D **78**, 50 (2024)
20. V. Sonnenschein, I.D. Moore, S. Raeder, M. Reponen, H. Tomita, K. Wendt, Laser Phys **27**, 085701 (2017)
21. V. Sonnenschein, H. Tomita, K. Kotaro, H. Koya, D. Studer, R. Terabayashi, F. Weber, K. Wendt, N. Nishizawa, T. Iguchi, Hyperfine Interactions **241**, 32 (2020)
22. V. Sonnenschein, M. Ohashi, H. Tomita, T. Iguchi, Nuclear Instruments and Methods in Physics Research Section B: Beam Interactions with Materials and Atoms **463**, 512 (2020)
23. D. Studer, J. Ulrich, S. Braccini, T.S. Carzaniga, R. Dressler, K. Eberhardt, R. Heinke, U. Köster, S. Raeder, K. Wendt, Euro. Phys. J. A **56**, 69 (2020)
24. S. Rothe, B.A. Marsh, C. Mattolat, V.N. Fedosseev, K. Wendt, J. Phys. **312**, 052020 (2011)
25. B. van den Borne, W. Gins, *Satlas2 – statistical analysis toolbox for laser spectroscopy, version 2*, https://iks-nm.github.io/satlas2/index.html, accessed: (2023)-10-23

26. W. Gins, R. de Groote, M. Bissell, C. Granados Buitrago, R. Ferrer, K. Lynch, G. Neyens, S. Sels, Comput. Phys. Commun. **222**, 286 (2018)
27. C. Günther, D.R. Parsignault, Nucl. Phys. A **104**, 588 (1967)
28. N. Stone, Atomic. Data Nucl. Data Tables **90**, 75 (2005)
29. W.B. Lewis, J.B. Mann, D.A. Liberman, D.T. Cromer, J. Chem. Phys. **53**, 809 (1970)
30. C. De Laat, A. Taal, W. Duinker, J. Konijn, J. Van Enschut, P. David, J. Hartfiel, H. Janszen, T. Mayer-Kuckuk, R. Von Mutius et al., Phys. Lett. B **189**, 7 (1987)